CRITICAL SCATTERING

W.G. STIRLING
Department of Physics, Oliver Lodge Laboratory,
The University of Liverpool,
Oxford St.,
LIVERPOOL L69 3BX, UK.

and

S.C. PERRY
Department of Physics, Keele University,
KEELE, Staffs ST5 5BG, UK.

ABSTRACT

We outline the theoretical and experimental background to neutron scattering studies of critical phenomena at magnetic and structural phase transitions. The displacive phase transition of $SrTiO_3$ is discussed, along with examples from recent work on magnetic materials from the rare-earth (Ho, Dy) and actinide (NpAs, NpSb, USb) classes. The impact of synchrotron x-ray scattering is discussed in conclusion.

1. Introduction and background theory

In this article we consider how neutron (elastic) diffraction and neutron (inelastic) scattering are used to give us unique information on phase changes in materials. This has been one of the most influential fields of neutron research with impact spreading far beyond the original experiments. Since we can only outline the theoretical and experimental background to this important area of neutron scattering research, we refer the reader to specialised texts. For a general introduction to the thermodynamics of phase transitions there are many excellent undergraduate text-books such as that by Adkins [1]. More specialised texts on critical phenomena in general include Stanley [2] and Yeomans [3]. For a detailed treatment of the relevant neutron techniques see the book on *Magnetic Critical Scattering* by Collins [4] and the article by Cowley [5].

A phase transition may usually be thought of as a change in the properties of a substance. Examples of everyday phase transitions are the change from ice to liquid water (melting), or the boiling of water to form steam (evaporation). These are called **first order** phase transitions, because the first derivative of the Gibbs function is discontinuous at the phase boundary. There are discontinuities in the entropy and volume at such a change of phase; hence there is always latent heat associated with a first order phase transition (the Clausius-Clapeyron equation).

If we consider the case of the pressure versus temperature phase diagram of a "simple" substance, Fig. 1, we notice that the boundary between the solid and liquid phases is always well-defined, while the phase boundary between the liquid and vapour phases terminates at a specific point, the critical point, beyond which it is possible to pass continuously from liquid to vapour phases, and *vice versa*. A phase transition which

passes directly through the critical point is known as a **higher order or continuous** phase transition; there is no discontinuity in the first derivative of the free energy and no latent heat associated with the transformation. The Ehrenfest classification scheme defines the order (first, second,...) of a transition to be the order of the lowest differential of the Gibbs function which exhibits a discontinuity at the transition. In practice **"second order transitions"** often display weak first order character very close to the actual transition. For our simple substance, at temperatures below the critical point there is a difference in the densities of the two phases, but this difference falls to zero as the critical point is approached. The density difference between the liquid and vapour phases can be used to characterise the transition and is known as the **order parameter** of the transition.

An analogy to the liquid-gas transition is the change in the magnetic properties of a magnetic substance as the temperature is lowered in zero applied field. An example is the change of the magnetic properties of Fe, which is paramagnetic above its Curie temperature (1043 K) and ferromagnetic below it. In zero applied field there is a continuous transition from one phase to the other. The order parameter of this transition is the **spontaneous magnetisation (M)**. In the case of antiferromagnets, the total magnetisation is zero above and below the transition, and the order parameter is the magnetisation for moments pointing in a specific direction, the **sublattice magnetisation**. Other examples of phase transitions and their associated order parameters are listed below:

Transition type	**Example**	**Order Parameter**
Structural	$SrTiO_3$	Rotation of oxygen octahedra
Order-disorder	CuZn	Sublattice atomic concentration
Ferroelectric	$BaTiO_3$	Electric polarisation
Superfluid	^{4}He liquid	Condensate wavefunction
Superconducting	Nb_3Sn	Ground state wavefunction

Consider the very over simplified 2 D model of a ferromagnet shown in Fig. 2. Well above the critical point T_C, in the paramagnetic phase,the elementary spins point in random directions; there is no sign of any (directional) magnetic order. So we have no **long range order** and little sign of **short range order** either. If we wish to identify a **length scale** to characterise this array of spins we are forced to choose the lattice parameter, a. At very low temperatures, well below T_C, things are equally clear. The strong ferromagnetic coupling aligns nearly all the spins in the same direction, and there is now strong long range order (technically infinite at T=O). Our characteristic length scale now measures regions of **deviation** from the prevailing spin direction, and falls to zero as $T \rightarrow 0$. Closer to T_C the situation becomes more interesting. Because there is no latent heat associated with a continuous transition the entropy difference between the two phases is quite small and so **statistical fluctuations** tend to give rise to short-lived regions of one phase in the other. As the critical point is approached the entropy difference decreases further and the length (and time) scales of the fluctuations increase. Thus the characteristic length increases and diverges as we get closer and closer to the transition temperature.

The longest length scale over which these regions exist is (roughly speaking) defined to be the **correlation length,** ξ; this becomes infinite at the critical point. It is important to realise that, although the longest length scale becomes infinite at T_C (extends over the entire volume of the system in reality), regions of correlated order still exist on

all other length scales, so that we have smaller regions of order **within** larger ones. At T_C there is no net magnetic moment, and there are exactly the same number of spins in all the allowed directions. A more accurate definition of the correlation length comes from introducing the pair correlation function $G(\mathbf{r},t)$ which describes the correlation of magnetic moments as a function of distance and time. Since much of our interest involves static correlations (time **in**dependent) we can often consider the static pair correlation function $G(\mathbf{r})$. The correlation length may be defined as the root-mean-square average of this function. In reciprocal space the corresponding quantity is the **inverse correlation length,** $\kappa = 1/\xi$.

What does all this mean for a neutron scattering experiment? As we approach the transition from above, the growth of the ordered regions will give rise to an increasingly intense signal, centered on the wavevector corresponding to the low-temperature ordered structure. The width of this "diffuse" peak will decrease as the correlation length increases and the inverse correlation length κ (in **Q**-space) correspondingly decreases. At the transition to a long-range ordered structure a **Bragg peak** of (theoretically) zero width begins to grow in intensity as the temperature is further lowered. We now consider this more formally. The neutron scattering intensity at a particular reduced wavevector $\mathbf{q}$ is proportional to the dynamic structure factor $S(\mathbf{q},\omega)$. If the scattering is properly integrated over all energies then the intensity of elastic scattering, the static structure factor $S(\mathbf{q})$, is simply proportional to the Fourier transform of the static correlation function:

$$S(\mathbf{q}) \sim \int \exp\text{-}i(\mathbf{q}.\mathbf{r})G(\mathbf{r})d\mathbf{r} \qquad (1)$$

Ornstein and Zernike [4] have proposed a useful approximation for the form of $G(\mathbf{r})$, by expanding it in a Taylor series and neglecting higher-order terms. This produces

$$G(\mathbf{r}) \sim \exp(\mathbf{r}/\xi)/\mathbf{r}^{d-2} \qquad (2)$$

where d is the spatial dimensionality of the system and ξ is the correlation length. We see that the correlations fall off faster than exponentially with distance and are infinite at r=0. The Fourier transform of this gives

$$S(\mathbf{q}) \sim 1/(1/\xi^2 + \mathbf{q}^2) \qquad (3)$$

which is a **Lorentzian** scattering function. This is an extremely useful form and has been shown to give an excellent representation of the critical scattering close to many different types of phase transition. We can also express the scattering in terms of the static susceptibility $\chi(\mathbf{q})$ when

$$\chi(\mathbf{q}) = \chi(0)/(1 + (\mathbf{q}/\kappa)^2) \qquad (4)$$

where $\chi(0)$ is the static susceptibility at $\mathbf{q} = 0$. Where the correlation lengths are not isotropic (the general case) this can be extended to

$$\chi(\mathbf{q}) = \chi(0)/(1 + (q_x/\kappa_x)^2 + (q_y/\kappa_y)^2 + (q_z/\kappa_z)^2)) \qquad (5)$$

where κ_x is the inverse correlation length for the x-direction, etc. When considering dynamic effects a related Lorentzian function can be used to describe the frequency widths,

$$\Gamma(\mathbf{q}) = \Gamma(0)/(1 + (q_x/\kappa_x)^2 + (q_y/\kappa_y)^2 + (q_z/\kappa_z)^2)) \quad (6)$$

where $\Gamma(\mathbf{q})$ is the characteristic frequency which appears in the dynamic structure factor $S(\mathbf{Q},\omega)$ or the closely related dynamic susceptibility $\chi(\mathbf{Q},\omega)$.

What is the interest in obtaining these quantities describing the growth of spatial and temporal correlations? An exciting feature of critical phenomena is the concept of **universality** [4]. The basic idea of critical phenomena is that the parameters describing phase transitions (the correlation lengths, the susceptibility, etc.) can be described by **power laws** in terms of the **reduced temperature**

$$t = (T - T_C)/T_C \quad (7)$$

such as

$$\kappa(T) = \kappa(0)\ |t|^{-\nu} \quad (8)$$

or

$$\chi(T) = \chi(0)\ |t|^{\gamma} \quad (9)$$

The quantities ν, γ,... are known as the **critical exponents** and there are certain relationships, equalities and inequalities, which connect them. The idea of universality is that the critical exponents do **not** depend on the specific details of the system (whether it is a magnetic or an order-disorder transition etc) but rather are governed by a few **general** properties, the **dimensionality** d of the system, the **symmetry** of the order parameter and the **long-or-short range nature** of the interactions. These powerful generalisations permit very detailed predictions to be made about the critical behaviour of a particular system. A more detailed analysis is beyond the scope of this article; for further information we refer the reader to references [2] to [4].

2. Experimental Issues

Here we discuss a few important experimental points. For more complete treatments see references [4] and [5]. The most flexible neutron scattering instrument and consequently the most useful for critical scattering studies is the triple-axis crystal spectrometer (TAS) [6]. A schematic diagram is given in Fig. 3. A particular incident neutron energy E is selected from the "white" beam from the reactor by the monochromator crystal **M**, normally a metal single-crystal (Cu(111), Al(002),...) or pyrolytic graphite (002). The scattering by the sample (**S**) is analysed in both energy and direction by the analyser/detector (**A/D**) system. Soller slit collimators are placed before and after each element. The power of this technique resides in its ability to probe specified regions of $(\mathbf{Q},\omega)$ space with flexibility in energy transfer and instrumental resolution. Although it is almost 40 years since Brockhouse and colleagues built the first

TAS instrument at Chalk River, all major reactor centres operate such instruments which are still responsible for many major scientific advances.

For studies of critical scattering which is localised near an ordering wavevector, is quasi-elastic (centred on zero energy transfer), and "sharpens" in both E ansd **Q** as the transition is approached, the TAS instrument is unrivalled. Suitable choice of incident and scattered energies, of collimations and monochromator/analyser crystals allows the instrumental component of the observed scattering. A detailed knowledge of the instrumental resolution function is an essential prerequisite for a correct analysis of critical scattering data. Critical scattering peaks are often barely wider than the instrumental contribution, which is normally Gaussian to a good approximation. It is essential to (de)convolute the data correctly, taking proper account of instrumental effects. The method of Cooper and Nathans [7] is still used extensively, although sophisticated numerical integration techniques are employed to carry out the integrations over the 3 dimensions of **Q** and the 4th E dimension of the resolution ellipsoid.

Fig. 4 presents some idealised lineshapes in which model Lorentzian functions representing the "physics", whose widths change each time by a factor of 10, are convoluted with a Gaussian resolution function of fixed width. Notice how the width of the convoluted peak, which is what we measure, changes relatively little for the two narrowest Lorentzians. There is a major change in the width, however, when the Lorentzian becomes as wide or wider than the Gaussian. These 3 examples correspond roughly to the case of $T >> T_c$ for the widest peaks, $T > T_c$ for the middle case and $T \sim T_c$ for the narrowest. As a rule-of-thumb, if a reliable measurement (or calculation) of the resolution function is available it is usually possible to extract "physical" widths down to about 10-20% of the resolution width. This can be extended downwards if "physical" and resolution data of exceptional statistical quality are available.

When measuring **static** critical exponents care must be taken to ensure that the energy integration covers the full dynamic range of the critical fluctuations (if the resolution in energy is too good, then contributions outside the resolution ellipsoid will not be included, falsifying the results). Often this is achieved by measuring in 2-axis diffraction mode (without an analyser crystal) with a neutron energy sufficiently large to ensure a complete energy integration. The problems associated with satisfying this **quasi-elastic approximation** are discussed in detail in Cowley's article [5]. The fulfilment of this condition is not always a problem even with a triple-axis analyser, as shown by the neptunium antimonide experiments discussed below in Section 4.

Although TAS instruments are still employed for most critical scattering investigations other types of spectrometer are used, such as the neutron spin-echo instrument or various types of time-of-flight spectrometer [6]. Very promising results are being obtained by Hagen and collaborators using the PRISMA instrument [8] at the ISIS pulsed neutron source. A pulsed white beam is incident on the sample and the scattered energy is analysed by a bank of 16 single-crystal analysers. Thus 16 distinct trajectories are traced out simultaneously in ($\mathbf{Q}$, ω) space. Up to now only 4 detectors have been used, for static measurements without analysers, but a new 16-detector critical scattering bank is under development for both static and dynamic critical scattering.

3. Structural Phase Transitions; example, $SrTiO_3$

Strontium titanate has the simple cubic perovskite structure. The antiferrodistortive

transition at 105 - 110 K is one of the most studied solid state transitions. It is driven by the condensation of a "soft-mode" at the R-point (1/2,1/2,1/2) of the Brillouin zone. This antiferrodistortive transition involves rotations of the oxygen octahedra and it is this rotation angle which is the order parameter of the transition. Although much of the interest in this transition concerns the **dynamical** "central peak", for which no completely convincing explanation has been forthcoming, new investigations have been made at BNL [9,10] of the static critical scattering, motivated by intriguing x-ray results [11]. Fig.5 presents some typical elastic scans above T_C along the [h,1/2,1/2] direction. As the transition is approached the scattering gets stronger and narrower in agreement with the ideas outlined in Section 1. Convolution of a model scattering function, such as Eq. 3 or Eq. 5, with the resolution function of the instrument allows the correlation lengths at each temperature to be refined in a least-squares procedure. We shall return to $SrTiO_3$ in Section 5.

4. Magnetic Phase Transitions; examples, Ho, Dy, NpAs, NpSb, USb.

Many elegant experiments have been carried out on magnetic ordering transitions. There have been several studies of the paramagnetic to helical magnetic phase transition in the **heavy rare-earth metals** holmium and dysprosium. In the helical antiferromagnetic phase the moments lie in the basal (ab) plane of the hexagonal structure and are strongly coupled ferromagnetically in this plane. Experiments at ORNL [12] have been motivated by conflicting theoretical predictions [13,14] for the critical exponents. In Fig. 6 we present typical lineshape data for Ho [12] taken for two orthogonal directions through the ordering wavevector $\mathbf{q}$ = (0,0,0.28). Critical behaviour (increased intensity and narrowing) is observed as the Néel point (T_N = 132.2 K) is approached. The critical scattering of both Ho and Dy is anisotropic as shown by the results of the fitting procedure (Fig. 7), using a variant of Eq. 5, where distinct inverse correlation lengths were obtained for the basal (ab) plane and c-direction. However, the power-law fits (e.g. Eq. 8 or 9) in terms of the reduced temperature (Eq. 7) are seen to correspond to very similar critical exponents, ν (i.e. the slopes of the log-log plots are the same within error). These new values agree well with the more recent theory [14] suggesting that Ho and Dy belong to a new universality class which includes 3D XY antiferromagnets with a layered triangular lattice.

We now consider a group of **actinide** antiferromagnets, starting with the exotic materials neptunium arsenide and neptunium antimonide. These are representatives of a class of actinide antiferromagnets with the simple rock-salt (NaCl) structure which exhibit a fascinating range of magnetic behaviour and structures. NpAs orders at T_N = 173.6 K into an incommensurate structure with an ordering wavevector of $\mathbf{q}$ = (0,0,0.23). This corresponds to a longitudinal magnetic modulation (with a repeat distance of 1/q ~ 4.3 unit cells) in which the spin direction is parallel to the propagation direction $\mathbf{q}$. The Np spins lie in sheets, stacked along the [0,0,1] direction. At lower temperatures (158.2 K and 140 K) there are other magnetic transitions. The anisotropic interactions in this nominally cubic structure are reflected in the anisotropy of the critical fluctuations [15] as exemplified by Fig. 8. Orthogonal scans made at ILL at T = 176.85 K are shown; the large anisotropy in the width, a factor of about 3, is evident. The corresponding inverse correlation lengths are also plotted in Fig. 8 (right-hand panel), corresponding to an exponent ν of 0.73, close to the theoretical 3D Heisenberg model value of 0.7. NpSb has a much simpler magnetic phase diagram with a single transition to a type-I

antiferromagnetic structure (i.e. **q** = [001]) at 199 K. Similar data to those of Fig. 8 are presented in Fig. 9 [15] where once again the anisotropy in the critical scattering is obvious. The right-hand panel of this figure shows how the integrated intensity of the (110) magnetic Bragg peak varies with temperature below T_N. The two different lines were obtained with (lower) and without (upper) an analyser crystal. The fact that the lines are parallel means that the intensity exponent β is the same from the 2-axis and 3-axis measurements. Hence the quasi-elastic approximation (Section 2) was satisfied as the energy width of the critical fluctuations was very small. In fact this last point was verified directly by making energy scans.

To conclude this section we consider uranium antimonide, the subject of a number of neutron investigations of spin structures and dynamics. USb also has the rock-salt structure and orders antiferromagnetically at 212.5 K into a (triple-**q**) type I structure. Examples of the critical scattering observed at ORNL [16] are given in Fig. 10 where the left-hand curves are wavevector scans while those on the right are energy scans, probing the dynamics of the critical fluctuations. The resulting power-law plots are shown in Fig. 11. The upper two lines are the inverse correlation lengths κ_x in direction [110] and κ_y in the orthogonal direction [001]. They are seen to be different, reflecting again the anisotropic magnetic interactions, but have similar critical exponents ν of about 0.7. The lower curve is the characteristic frequency (Eq. 6) with exponent Δ of 1.6. These are close to the 3D Heisenberg values.

5. Concluding Remarks

From the above it might appear that everything is understood about phase transitions, that in general the experimental exponents are in accord with the most modern theory, and that all the excitement has gone. This is not the case! Our acceptance that phase transitions are well understood has been challenged by a series of puzzling observations made using **x-ray** diffraction. In a series of laboratory experiments in the mid 80s Cowley, Nelmes and their collaborators in Edinburgh discovered that the static critical scattering lieshapes at structural phase transitions in perovskites (such as $SrTiO_3$, introduced in Section 3) could not be described in terms of a single correlation length. This was followed up by synchrotron radiation studies where the very high wavevector resolution allowed a clear separation into sharp and wide components. Fig. 12 shows a "two-component" lineshape observed by synchrotron x-ray diffraction [11] compared with a comparable neutron scan which only exhibits a single (relatively) broad peak. More recently such double peaks were observed at **magnetic** transitions in synchrotron magnetic scattering experiments. A good example is given in Fig. 13 for USb [17]. The broad component is described by the exponent derived from the neutron experiments [16], but the sharp component is also "critical" (with a very similar transition temperature) but with a very different exponent. Very high resolution **neutron** scattering has shown up double-peak critical scattering in holmium [18]. The origin of the extra sharp peak is still unclear, but it appears that strains in the near-surface region are involved. This work has led to a resurgence of interest in phase transitions and a reassessment of "standard" theory. There is a bright future for neutron scattering as this recent work has shown that the combination of neutron and x-ray results is a very powerful tool for the study of phase transitions.

6. Acknowledgements

We are especially grateful to Dr. M.E. Hagen and Prof. G.H. Lander whose work we discuss in this article and to all the colleagues who helped with our neutron scattering experiments at various reactor centres. SCP thanks the EPSRC for the award of a PhD studentship.

7. References

1. C.J. Adkins, *Equilibrium Thermodynamics* (Cambridge University Press, 1989).
2. H.E. Stanley, *Introduction to Phase Transitions and Critical Phenomena* (Oxford University Press, 1971).
3. J.M. Yeomans, *Statistical Mechanics of Phase Transitions* (Oxford University Press, 1992).
4. M.R. Collins, *Magnetic Critical Scattering* (Oxford University Press, 1989).
5. R.A. Cowley, in *Methods of Experimental Physics, Vol. 23 part C, Neutron Scattering*, eds. K. Skold and D.L.Price (Academic Press Inc, 1986).
6. C.G. Windsor in *Methods of Experimental Physics, Vol. 23 part A, Neutron Scattering*, eds. K. Skold and D.L.Price (Academic Press Inc, 1986).
7. M.J. Cooper and R. Nathans, *Acta Crystallogr.* **23** (1967) 257.
8. S.J. Payne, M.E. Hagen, and M.J. Harris, *J. Phys.: Condens. Matter* **8** (1996) 91.
9. G. Shirane, R.A. Cowley, M. Matsuda and S.M. Shapiro, *Phys. Rev.* **B48** (1993) 15595.
10. K. Hirota, J.P. Hill, S.M. Shapiro, G. Shirane, and Y. Fujii, *Phys. Rev.* **B52** (1995) 13195.
11. D.F. McMorrow, N. Hamaya, S. Shimomura, Y. Fujii, S. Kishimoto and H. Iwasaki, *Solid State Commun.* **76** (1990) 443; and references therein.
12. B.D. Gaulin, M.E. Hagen and H.R. Child, *J. de Phys.* **49** (1988) C8-327.
13. P. Bak and D. Mukamel, *Phys. Rev.* **B13** (1976) 5086.
14. H. Kawamura, *J. Appl. Phys.* **63** (1988) 3086.
15. D.L. Jones, W.G. Stirling, G.H. Lander, J. Rebizant, J.C. Spirlet, M. Alba and O. Vogt, *J. Phys.: Condens. Matter* **3** (1991) 3551.
16. M.E. Hagen, W.G. Stirling and G.H. Lander, *Phys. Rev.* **B37** (1988) 1846.
17. S.C. Perry, W.J. Nuttall, W.G. Stirling, G.H. Lander and O. Vogt, *Phys. Rev.* **B** in press.
18. T.R. Thurston, G. Helgesen, D. Gibbs, J.P. Hill, B.D. Gaulin and G. Shirane, *Phys. Rev. Letters* **70** (1993) 3151.

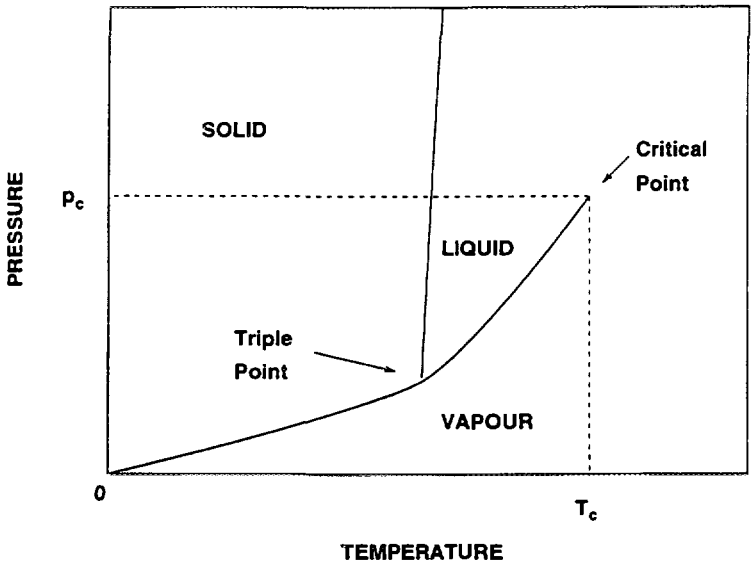

1. Pressure-temperature phase diagram of a simple substance. The triple point and critical point T_C are marked.

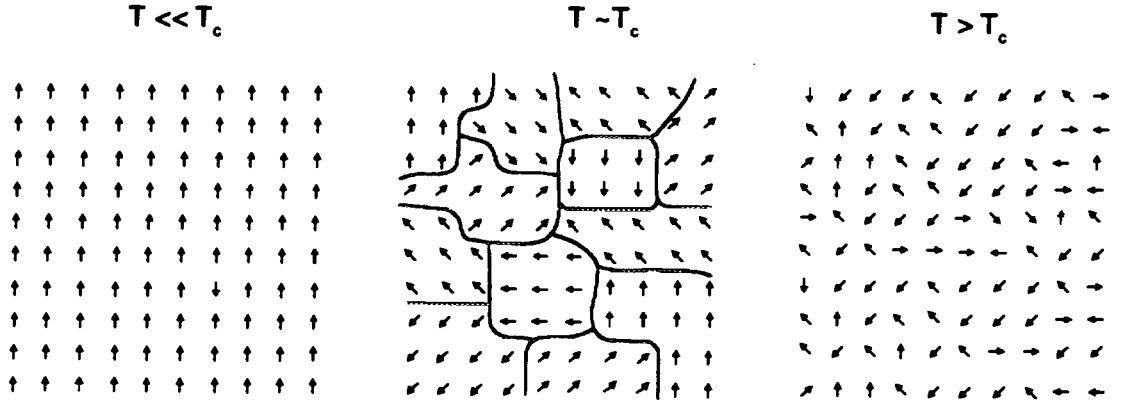

2. Schematic diagram of a simple 2D magnet showing the growth of ordered regions near T_C.

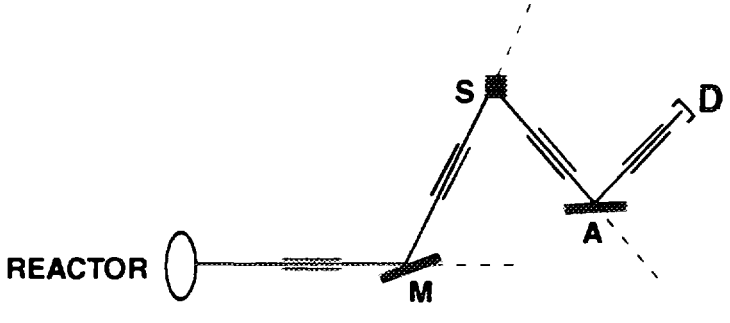

3. Schematic diagram of a triple-axis crystal spectrometer.

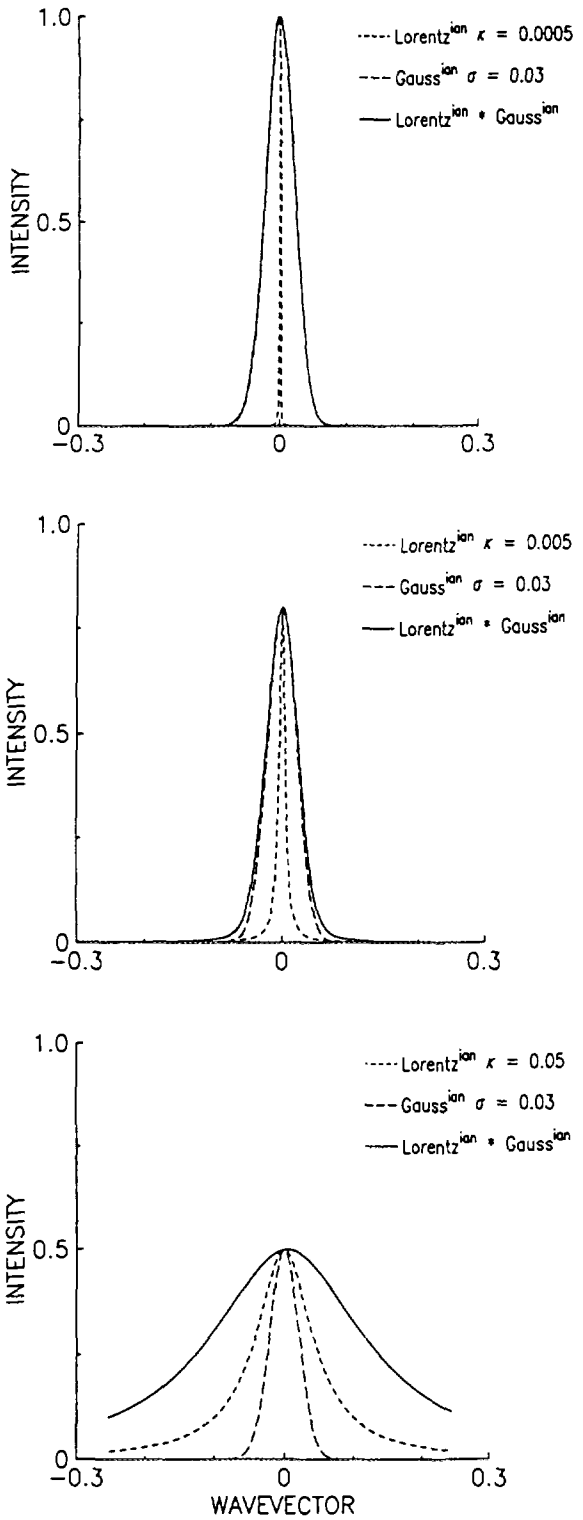

4. Examples of convolutions of a Gaussian function of fixed width (representing the instrumental resolution) with Lorentzian functions of varying width (representing the "physics").

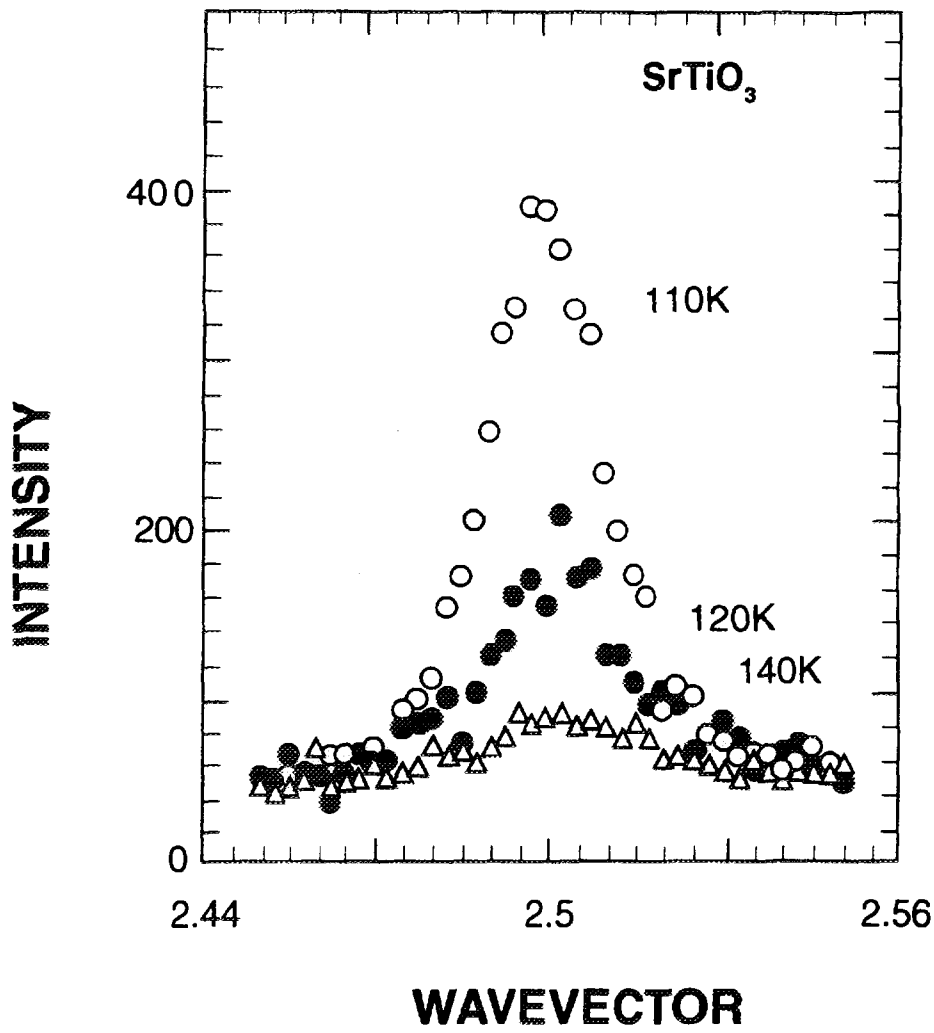

5. Critical scattering in $SrTiO_3$ for the [h,0.5,0.5] direction. Open circles, 110 K, closed circles, 120 K, triangles, 140 K. After ref. [10].

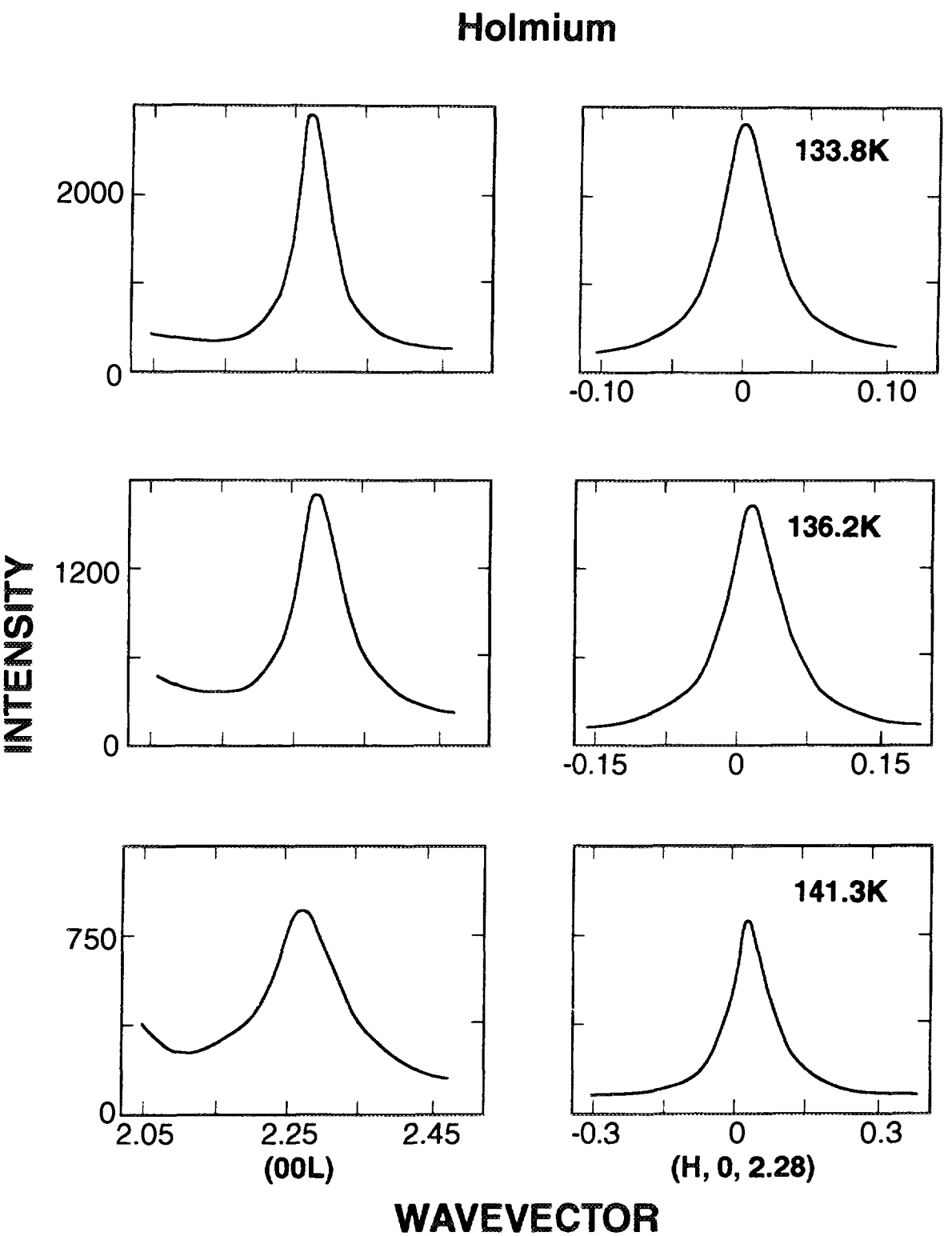

6. Critical magnetic scattering lineshapes for Ho for two orthogonal directions. After ref. [12].

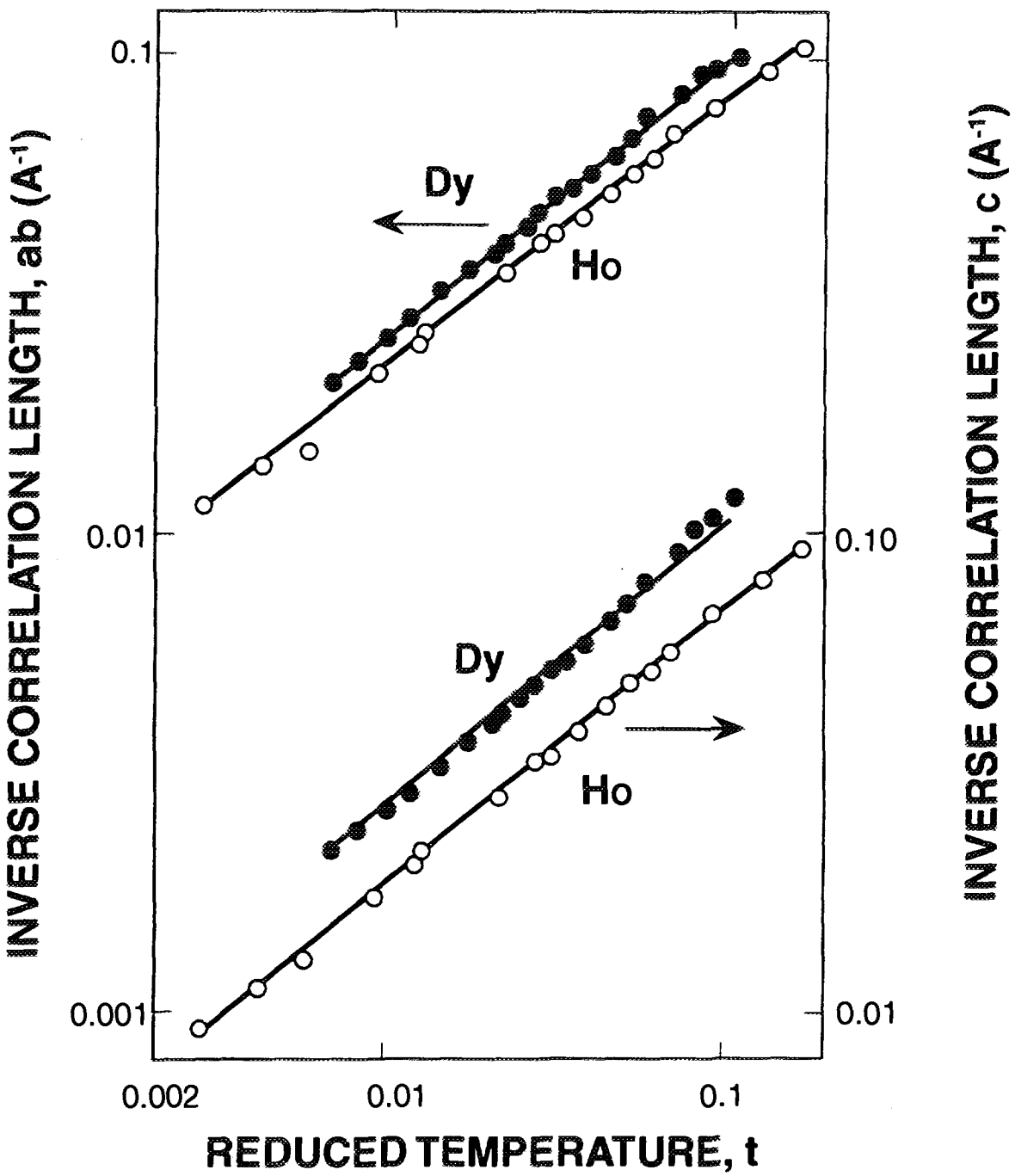

7. Power-law fits of inverse correlation lengths in the basal plane (ab) and c-direction of Ho and Dy. After ref. [12].

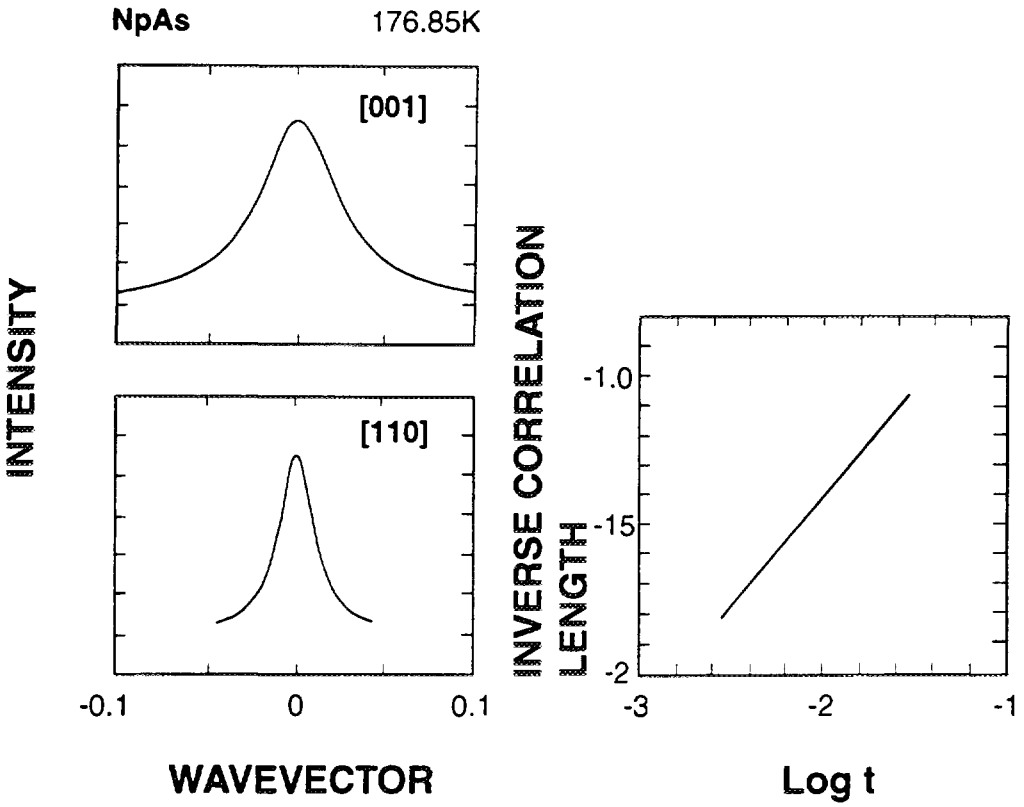

8. Left: critical scattering lineshapes of NpAs demonstrating the anisotropic critical fluctuations. Right: power-law fit to inverse correlation lengths. After ref. [15].

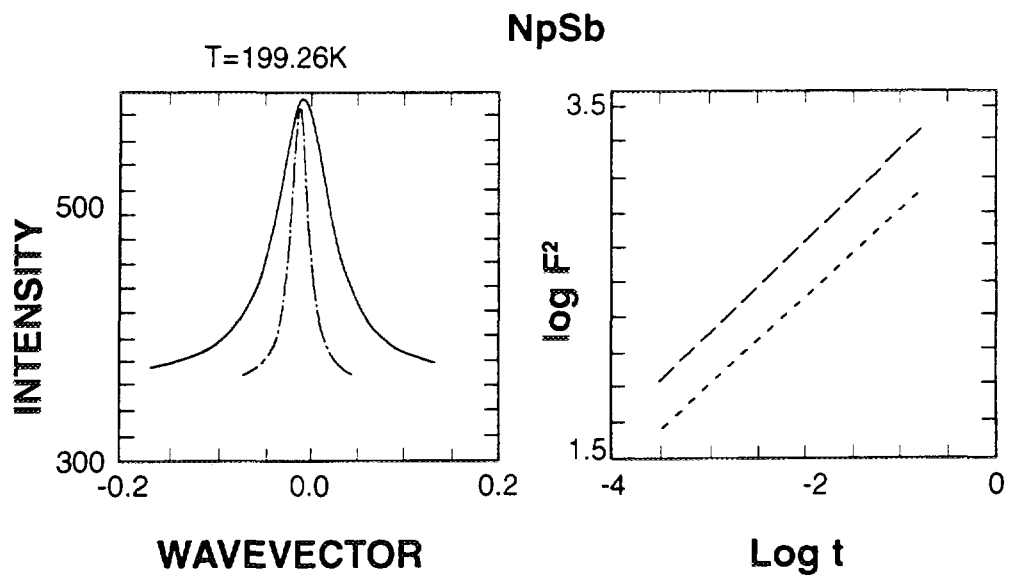

9. Left: anisotropic critical scattering of NpSb.
Right: Integrated intensity (F^2) of the (110) Bragg peak below T_N. Upper line, without analyser; lower line, with analyser. After ref. [15].

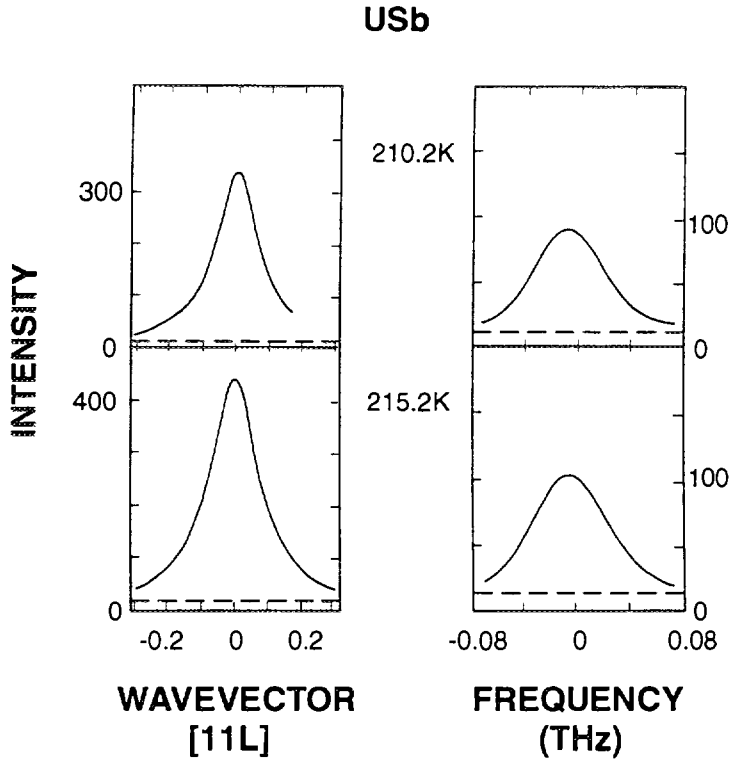

10. Critical scattering above T_N of USb. Right: wavevector scans. Left: frequency scans. After ref. [16].

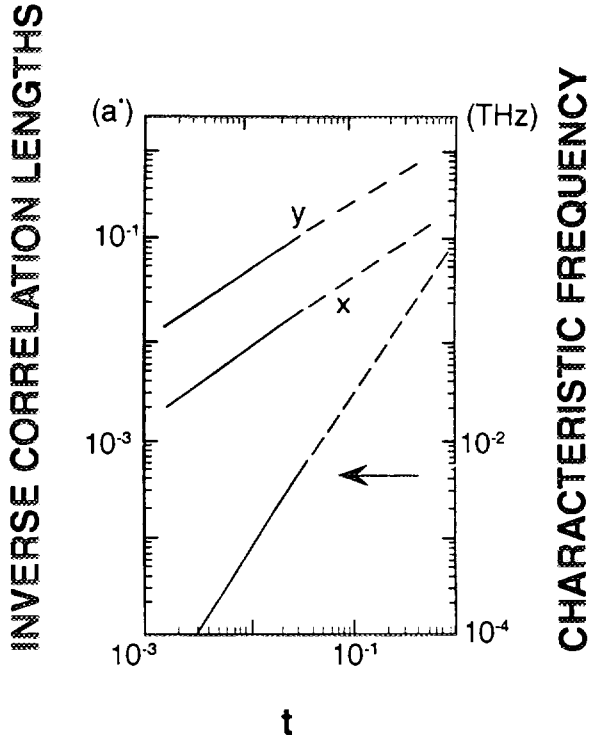

11. Power-law fits for USb to inverse correlation lengths and characteristic frequency. After ref. [16].

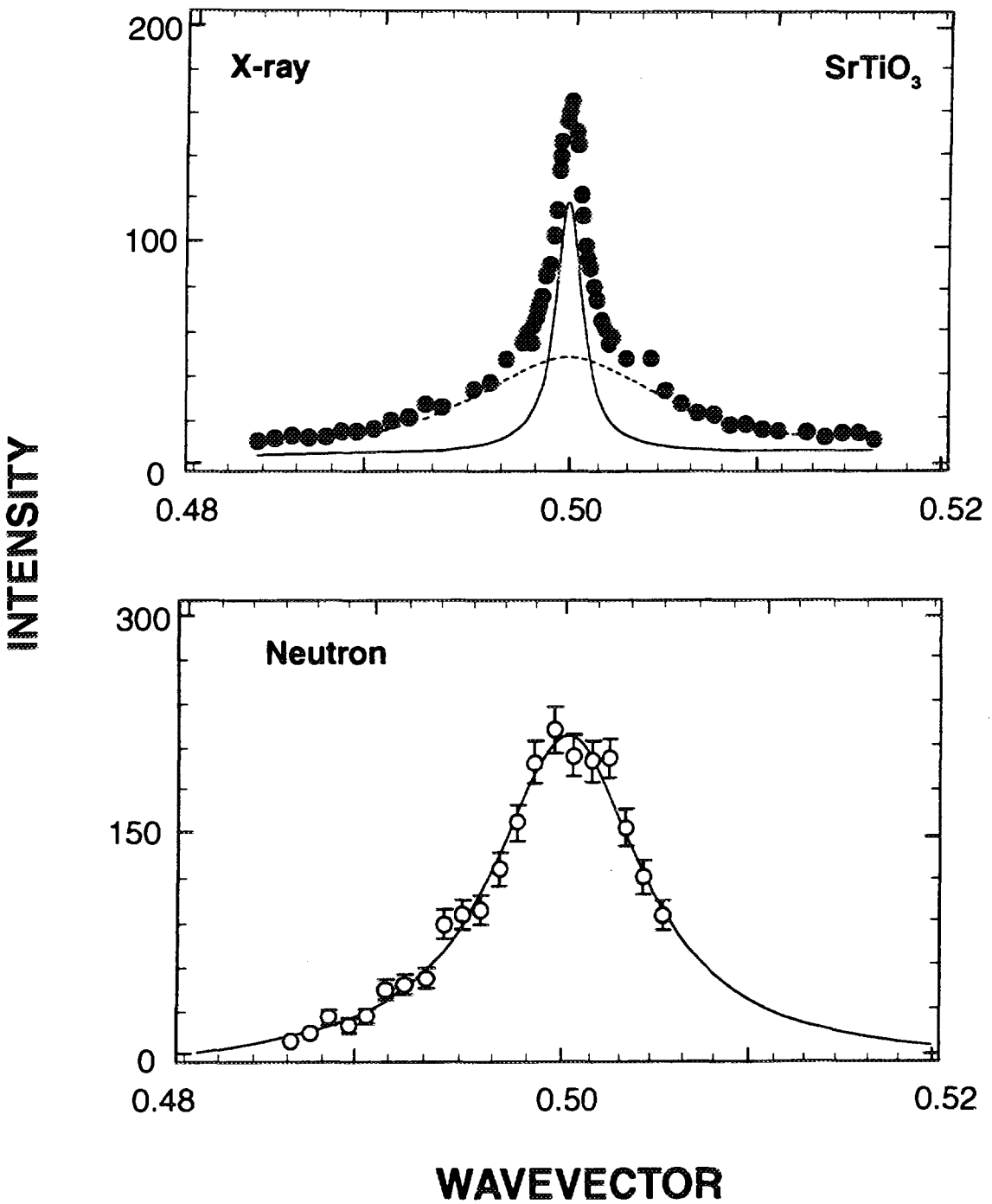

12. Comparison of x-ray and neutron lineshapes for $SrTiO_3$. After refs. [10] and [11].

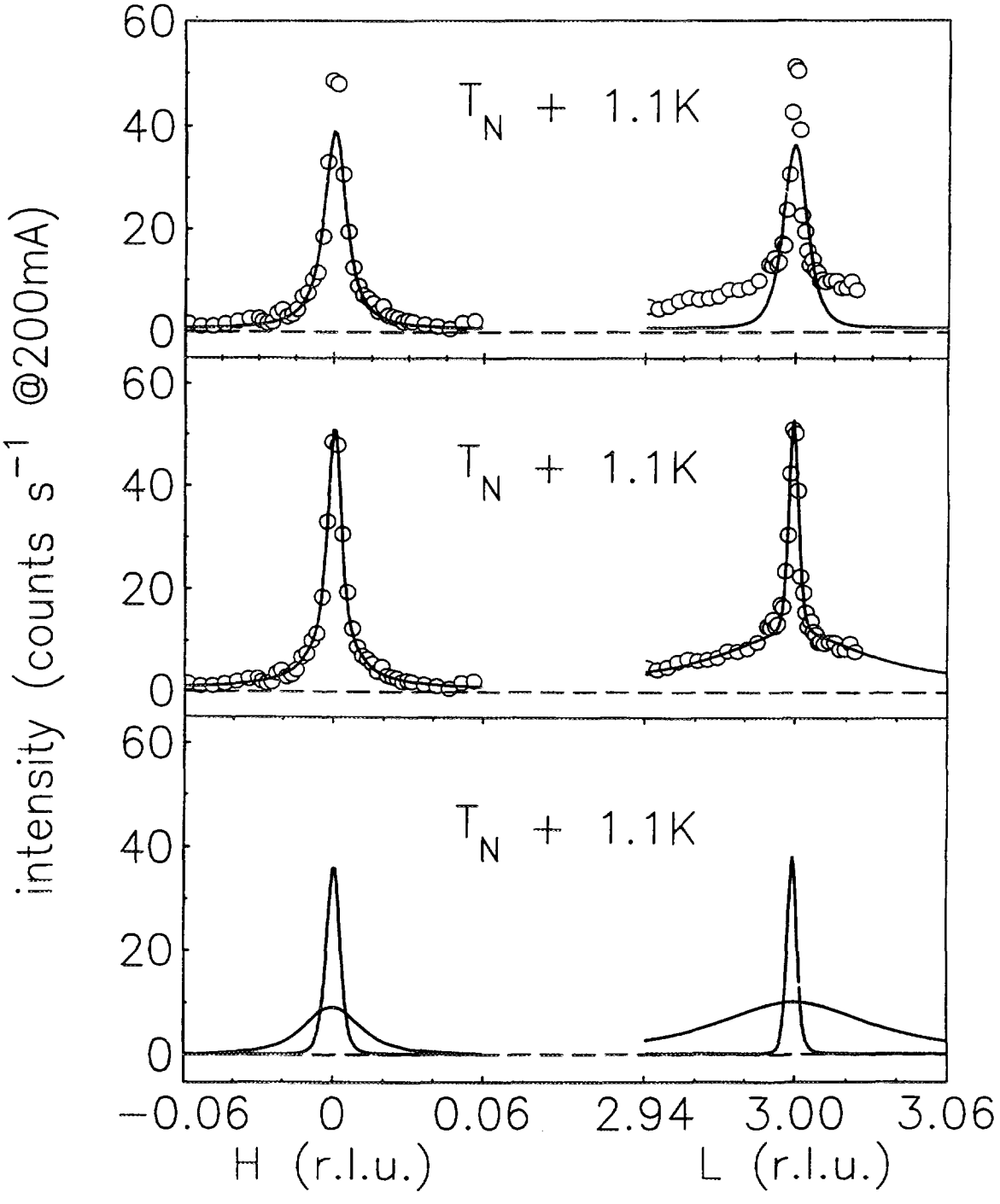

13. Two-component x-ray lineshapes of USb. Upper panel, comparison with single Lorentzian fit. Middle panel, fit to sum of Lorentzian plus Lorentzian-squared. Lower panel, components of $L + L^2$ model. After ref. [17].